Meso-Beta Scale Numerical Simulation Studies of Terrain-Induced Jet Streak Mass/Momentum Perturbations

FY94 November Annual Report

submitted to the

Mesoscale Processes Research Program

Atmospheric Dynamics and Radiation Branch

Earth Science and Application Division

Office of Space Science and Applications

NASA Headquarters

Washington, D. C. 20546

Attention: Dr. Ramish Kakar, Program Manager

by

Yuh-Lang Lin and Michael L. Kaplan

Department of Marine, Earth, and Atmospheric Sciences

North Carolina State University

Raleigh, North Carolina 27695-8208

(919) 515-1438

November 1994

Table of Contents

Part I: 3-D Numerical Modeling of Meso-Beta Scale Terrain-Induced Jet Streak Mass/Momentum Adjustments

1. Introduction

Recently, Koch and Dorian (1988) produced an in-depth analysis of observed gravity waves and their relationship to precipitation bands over the Montana mesonetwork during the 11-12 July 1981 CCOPE case study. Their analyses indicated two episodes of coherent internal gravity waves. One of the fundamental unanswered questions from this research, however, concerns the dynamical processes which generated the observed waves, all of which originated from the region encompassing the borders of Montana, Idaho, and Wyoming. While geostrophic adjustment, shearing instability, and terrain where all implicated separately or in concert as possible wave generation mechanisms, the lack of upper-air data within the Wave Genesis Region (WGR, Fig. 1) made it difficult to rigorously define the genesis processes from observations alone. In this report we employ a mesoscale numerical model to help diagnose the intricate early wave generation mechanisms during the first observed wave episode.

2. Synoptic-Scale Observations

At 0000 UTC 11 July 1981 a massive ridge of high pressure covered most of the western Great Plains and inter mountain region of the U. S. and southwestern Canada, while a cutoff low was located over coastal Washington (not shown). In between, the polar jet streak stretched from northern California to southwestern Saskatchewan with its right exit region over western Montana. The inflection point in the ridge was in proximity to the right exit region of the jet streak. Also evident from individual wind component analyses and satellite imagery (not shown) is the development of a secondary jet streak structure some 200-300 km to the southeast of the primary jet during the 0000-1200 UTC time period. In addition, a weak short wave trough is observed to intensify over western Montana by 1200 UTC as it propagates northeastwards, during which time the low-level wind flow accelerates towards the north over the WGR.

3. Numerical Experiments

The hydrostatic numerical model employed for the simulation experiments is the GMASS model (Manobianco *et al.*, 1994). A matrix of 223 x 146 x 30 grid points was centered over the northern Rocky Mountain region with ~16 km horizontal resolution while an identical nested grid matrix was centered over west-central Montana with ~8 km horizontal resolution. The coarse mesh simulation was initialized at 0000 UTC 11 July 1981 from standard LFM analysis data, rawinsondes, and surface observations and integrated through 0600 UTC 12 July 1981. The nested-grid simulation was initialized at 0900 UTC 11 July 1981 and integrated through 0600 UTC 12 July 1981. Initial and boundary conditions for the nested-grid were derived from the coarse mesh simulation. While several physics and terrain sensitivity experiments have been performed, for brevity we will only compare a coarse mesh constant terrain elevation simulation in the absence of latent heating (simulation A) and a nested-grid high resolution terrain simulation also with latent heating supressed (simulation B) to diagnose the geostrophic adjustment process(es) which contribute(s) to the organization of the first observed gravity wave episode which develops shortly after 1200 UTC on 11 July 1981.

4. Primary Geostrophic Adjustment Period

Figure 1 depicts the simulation A sequence of 500 mb wind vectors and isotachs during the 0000-0600 UTC time period. Evident is a dramatic modification of the jet exit region structure as the velocity maximum over west central Idaho at 0000 UTC encounters the changing pressure gradient force over western Montana. By 0300 UTC (not shown) a secondary velocity maximum (J_2 in Fig. 1b) develops to the north of the 0000 UTC maximum. This secondary maximum is the result of the increased cross-stream directed pressure gradient force encountered by air parcels exiting the jet over western Montana. This results in a local increase of the cross-stream wind velocity component. Three hours later, the inertial-advective terms in the equations of motion adjust to the northward acceleration by increasing the along-stream wind component

to the southeast of the secondary maximum. Thus, the rotational wind increases downstream over central Montana so that by 0600 UTC a new southeastward-shifted "jetlet" (J3) has formed, thus bifurcating the original jet structure. Therefore, the wind has geostrophically adjusted to the mass field forming a split jet streak structure just northwest of the WGR. This is consistent with satellite imagery showing a secondary cirrus plume over southeastern Idaho at 0600 UTC which redevelops northeastward to southwestern Montana by 0900 UTC (not shown).

5. Geostrophic Adjustment Frontogenesis

Consistent with the aforementioned adjustment process in simulation A is the development of a thermally-indirect circulation oriented both across and along the stream. This circulation is in response to the velocity divergence and convergence patterns accompanying the secondary "jetlet" formation northwest of the WGR. The mass field adjusts to the secondary jetlet by inducing midtropospheric ascent on the cyclonic and upstream side and midtropospheric descent on the anticyclonic and downstream side, resulting in adiabatic cooling and warming respectively, by 0500 UTC and frontogenesis northwest of the WGR during the 0200-0800 UTC time period (Figure 2).

6. Secondary Geostrophic Adjustment

The jetlet which induces the aforementioned frontogentical circulation propagates downstream over Montana during the 0800 UTC through 1200 UTC time period. At this time the new midtropospheric mass perturbation coupled to the aforementioned midtropospheric front induces a secondary geostrophic adjustment process to the south and east of the primary geostrophic adjustment, i. e., near the WGR. By 1300 UTC the simulation A 500 mb winds and vertical motions (Figure 3) indicate that this secondary jetlet's exit region has produced an along-stream thermally-indirect circulation along the southeastern periphery of the previous jetlet's circulation, thus resulting in ascent, saturation, and velocity divergence directly over the WGR at the time of the initial gravity wave generation. The flow in this region at this time is highly

ageostrophic and unbalanced. Beneath the midtropospheric circulation can be seen the exit region of a newly-formed 700 mb low-level jet (LLJ) which has been induced by the enhanced height falls just upstream from the WGR under the secondary midtropospheric jetlet and in proximity to the propagating low-level short wave trough. The existence of a localized pattern of relative humidity near the WGR (not shown) forced by the convergence accompanying the LLJ is consistent with the development of convection and the first gravity wave episode, both of which are observed to commence at approximately 1300 UTC.

7. Genesis of Internal Gravity Waves

Figure 4 depicts the generation of internal gravity waves by simulation B. These features, evident in the 500 mb vertical velocity field have a wavelength consistent with the primary modes observed by Koch and Dorian (1988), however they produce a weaker pressure signal and move somewhat slower. These waves are virtually absent in the coarse mesh simulations yet are somewhat stronger as the terrain resolution is enhanced. At this stage of the analysis of the various simulations it is evident that geostrophic adjustment is the physical mechanism which initiates the observed gravity waves, however, their amplification appears to be affected by latent heating and surface sensible heat flux.

8. Summary and Conclusions

The role of multiple geostrophic adjustment processes in focusing a region for gravity wave genesis has been studied with various simulations from a meso-beta scale numerical model. The focusing of wave genesis near in space and time to where it is observed is the result of the following sequence of processes: 1) a cross-stream acceleration of the wind field is followed by an along-stream acceleration within the exit region of a polar jet streak which encounters the inflection point in the height field, 2) the resulting wind pattern represents the bifurcation of the original jet streak into multiple jet maxima displaced to the southeast of the original maximum but still northwest of the WGR, 3) the velocity divergence patterns induce differential patterns

of ascent and descent both across and along the stream resulting in midtropospheric frontogenesis, 4) a second geostrophic adjustment process occurs further southeast of the front which was near the WGR, 5) the vertically integrated divergence produced by the secondary adjustment over the WGR modifies the mass field resulting in low-level jet formation, and 6) gravity waves radiate downstream towards the CCOPE mesonet region located in eastern Montana.

9. Acknowledgements

This work was funded under NASA Contract NAG5-1790. The authors wish to acknowledge Dr. Ramesh Kakar for his support and Mr. David Hamilton for his work on the figures. The computer time was provided by the North Carolina Supercomputing Center. Dr. Ahmet Aksakal of NASA/GSFC provided technical assistance with the GMASS model.

10. References

Koch, S. E., and R. E. Dorian, 1988: A mesoscale gravity wave event observed during CCOPE. Part III: Wave environment and probable source mechanisms. *Mon. Wea. Rev.*, **116**, 2571-2592.

Manobianco, J., S. E. Koch, V. M. Karyampudi, and A. J. Negri, 1994: The impact of assimilating satellite-derived precipitation rates on numerical simulations of the ERICA IOP 4 cyclone. *Mon. Wea. Rev.*, **122**, 341-365.

Part II: Linear Theory

1. Introduction

The response of non-resting rotating homogeneous and continuously stratified Boussinesq models of the terrestrial atmosphere to temporally impulsive and uniformly propagating three-dimensional localized zonal momentum sources representative of midlatitude jet streaks is

investigated. The methods of linear perturbation theory applied to the potential vorticity (PV) and wave field equations are used to study the geostrophic adjustment dynamics associated with the initial value problem imposed by the introduction of an ageostrophic zonal jet in a uniform geostrophically balanced barotropic flow, as well as the forced problem imposed by an external momentum forcing traveling at the speed $c < U$ within the basic state current. Effects of nonlinearity are investigated using simple numerical shallow water and continuously stratified primitive equation models. The total zonal and meridional wind perturbations are separated into geostrophic and ageostrophic components in order to define and follow the evolution of both the primary and secondary mesocirculations accompanying midlatitude jetogenesis forced by geostrophic adjustment processes.

This problem is addressed in order to help fill the gap in our understanding of the dynamics and structure of mesoscale inertia-gravity waves forced by geostrophic adjustment processes in simple two-dimensional quiescent current systems (Rossby, 1938; Cahn, 1945) and those produced by mesoscale numerical models simulating the orographic and diabatic perturbation of three-dimensional quasi-geostrophically balanced synoptic scale jet streaks associated with complex baroclinic severe storm producing environments (Kaplan *et al.*, 1994a, b).

For brevity only the theory governing and figures illustrating features of the small-amplitude response in a rotating Boussinesq atmosphere are presented here. Details concerning the response in a homogeneous atmosphere of finite depth as well as a more rigorous discussion of the continuously stratified response in both infinite and semi-infinite Boussinesq atmospheres can be found in Weglarz (1994).

2. Theory

The field equations governing small-amplitude baroclinic perturbations in a rotating Boussinesq atmosphere forced by zonal (F_x) and meridional (F_y) momentum sources, diabatic heating/cooling (Q), and shallow orography may be combined to yield the linearized potential vorticity and wave field equations, which may be written collectively as:

$$L\,\phi'(x,y,z,t) = S(x,y,z,t), \tag{1}$$

where $\phi' = q'$, $\mathbf{u}' = (u', v', w')$, p' or θ'; $q' = \zeta' + (f/\rho_0 N^2)\partial^2 p'/\partial z^2$ is the linearized PV, and where the differential operators L and inhomogeneous source terms $S(\mathbf{r},t)$ are defined as:

$$L = \begin{Bmatrix} \dfrac{\partial}{\partial t} + U\dfrac{\partial}{\partial x} + V\dfrac{\partial}{\partial y}, & \text{if } \phi' = q' \\ \left[\left(\dfrac{\partial}{\partial t} + U\dfrac{\partial}{\partial x} + V\dfrac{\partial}{\partial y}\right)^2 + f^2\right]\dfrac{\partial^2}{\partial z^2} + N^2\nabla_H^2, & \text{if } \phi' = \mathbf{u}', p', \theta' \end{Bmatrix}, \tag{2}$$

$$S(\mathbf{r},t) = \begin{Bmatrix} F_\zeta + \dfrac{f\,g}{N^2 c_p T_0}\dfrac{\partial Q}{\partial z}, & \text{if } \phi' = q' \\ -N^2\dfrac{\partial q'}{\partial y} + \dfrac{\partial^2}{\partial z^2}\left(\dfrac{DF_x}{Dt} + f\,F_y\right) - \dfrac{g}{c_p T_0}\dfrac{\partial^2 Q}{\partial z \partial x}, & \text{if } \phi' = u' \\ N^2\dfrac{\partial q'}{\partial x} + \dfrac{\partial^2}{\partial z^2}\left(\dfrac{DF_y}{Dt} - f\,F_x\right) - \dfrac{g}{c_p T_0}\dfrac{\partial^2 Q}{\partial z \partial y}, & \text{if } \phi' = v' \\ -\dfrac{\partial}{\partial z}\left(\dfrac{DF_\delta}{Dt} + f\,F_\zeta\right) + \dfrac{g}{c_p T_0}\nabla_H^2 Q, & \text{if } \phi' = w' \\ \rho_0\left[N^2(f\,q' + F_\delta) + \dfrac{g}{c_p T_0}\dfrac{D}{Dt}\dfrac{\partial Q}{\partial z}\right], & \text{if } \phi' = p' \\ \dfrac{\theta_0}{g}\dfrac{\partial}{\partial z}\left(\rho_0\left[N^2(f\,q' + F_\delta) + \dfrac{g}{c_p T_0}\dfrac{D}{Dt}\dfrac{\partial Q}{\partial z}\right]\right), & \text{if } \phi' = \theta' \end{Bmatrix}, \tag{3}$$

where $F_\zeta = \mathbf{k}\cdot\nabla\times\mathbf{F}$, $F_\delta = \nabla\cdot\mathbf{F}$, $\nabla^2_H = \partial^2/\partial x^2+\partial^2/\partial y^2$ is the two-dimensional horizontal Laplacian, and the other symbols carry their conventional meteorological and mathematical meanings.

2.1 Method of Solution

The Fourier transform of any dynamical field variable and its inverse in a vertically unbounded Boussinesq atmosphere may be defined by the integral pair

$$\hat{\phi}(\mathbf{k},t) = \frac{1}{(2\pi)^3}\int_{-\infty}^{\infty}\int_{-\infty}^{\infty}\int_{-\infty}^{\infty}\phi'(\mathbf{r},t)\, e^{-i\,\mathbf{k}\cdot\mathbf{r}}\, d\mathbf{r}, \tag{4}$$

$$\phi'(\mathbf{r},t) = \int_{-\infty}^{\infty}\int_{-\infty}^{\infty}\int_{-\infty}^{\infty}\hat{\phi}(\mathbf{k},t)\, e^{+i\,\mathbf{k}\cdot\mathbf{r}}\, d\mathbf{k}, \tag{5}$$

where $\mathbf{r} = (x,y,z)$, and $\mathbf{k} = (k,l,m)$. The Fourier transform of the linearized PV and wave field equations in the absence of diabatic and orographic forcing yield

$$\frac{\partial\hat{q}}{\partial t} + i\,\Omega\,\hat{q} = -\,i\,l\,\hat{F}_\xi, \tag{6}$$

$$\frac{\partial^2\hat{\phi}}{\partial t^2} + 2\,i\,\Omega\,\frac{\partial\hat{\phi}}{\partial t} + R(\mathbf{k})\hat{\phi} = \hat{S}_\xi(\mathbf{k},t), \tag{7}$$

where

$$R(\mathbf{k}) = f^2 + \frac{N^2}{m^2}\kappa^2 - \Omega^2, \tag{8}$$

$$\hat{S}_\xi(\mathbf{k},t) = \begin{Bmatrix} i\,(l\,\frac{N^2}{m^2}\,\hat{q} + \Omega\,\hat{F}_\xi), & \text{if } \hat{\phi} = \hat{u} \\ -i\,k\,\frac{N^2}{m^2}\,\hat{q} - f\,\hat{F}_\xi, & \text{if } \hat{\phi} = \hat{v} \\ [\frac{(l\,f - i\,k\,\Omega)}{m}]\,\hat{F}_\xi, & \text{if } \hat{\phi} = \hat{w} \\ -\rho_0\,\frac{N^2}{m^2}\,(f\,\hat{q} + i\,k\,\hat{F}_\xi), & \text{if } \hat{\phi} = \hat{p} \\ -i\,\theta_0\,\frac{N^2}{m\,g}\,(f\,\hat{q} + i\,k\,\hat{F}_\xi), & \text{if } \hat{\phi} = \hat{\theta} \end{Bmatrix}. \tag{9}$$

$\Omega = k(U\text{-}c) + lV$ is the relative wave frequency and F_ξ is the vorticity of the external momentum forcing in a frame of reference translating at the zonal speed c through the basic state flow. Note that in this frame the applied forcing is stationary. The general solutions to the forced linearized potential vorticity and wave field equations, Eqs. (6) and (7), respectively, are found to be:

$$\hat{q}(\mathbf{k},t) = [\hat{q}_i(\mathbf{k}) + \frac{1}{\Omega}\,\hat{F}_\xi(\mathbf{k})]\,e^{-i\,\Omega\,t} - \frac{1}{\Omega}\,\hat{F}_\xi(\mathbf{k}), \tag{10}$$

$$\hat{\phi} = A_\phi e^{+i\,\omega_-\,t} + B_\phi e^{-i\,\omega_+\,t} + C_\phi e^{-i\,\Omega\,t} + D_\phi. \tag{11}$$

The coefficients A_ϕ, B_ϕ, C_ϕ, and D_ϕ are determined by applying appropriate initial conditions to the initial value and forced geostrophic adjustment problems, respectively. Details can be found in Weglarz (1994). The frequencies of the transient dispersive inertia-gravity waves represented by the first two terms on the r.h.s. of Eq. (11) are given by:

$$\omega_{\pm} = \sqrt{f^2 + \frac{N^2\kappa^2}{m^2}} \pm \Omega \qquad (12)$$

3. Results

Fig. 5 shows the linear response at t = 6 h after the introduction of an ageostrophic zonal wind anomaly whose horizontal and vertical structure is specified to be:

$$u'_i = u'_{jet} = u_{j0} \left(\frac{x^2}{a^2} + \frac{y^2}{b^2} + 1\right)^{-3/2} e^{-z^2/d^2}. \qquad (13)$$

The zonal and meridional half-widths a, b are equal and taken to be 50 km, while the vertical e-folding half-depth d is taken to be 2.5 km. The magnitude of the unbalanced zonal jet u_{j0} is specified to be 20 ms^{-1}. The significant radius of deformation is defined by $L_R = N(2d)/f = 500$ km ($N = 10^{-2}$ s^{-1}, $f = 10^{-4}$ s^{-1}). Since $a = b = L_R/10 << L_R$, then the thermodynamic fields will tend to adjust to the rotational part of the initial wind field (Rossby, 1938; Cahn, 1945).

Horizontal cross sections of $\mathbf{u}' = (u', v', w')$ (Figs. 5a, b, and c) and p' (Fig. 5d) are shown at z = 0, the level at which the initial zonal wind anomaly is a maximum (Eq. 13). At this time, outwardly propagating inertia-gravity waves in both the perturbation wind and pressure fields are associated with the non-zero divergence tendency ($\partial\delta'/\partial t$) induced by the ageostrophic zonal jet. The magnitude of the initial jet has fallen to approximately 7.3 ms^{-1} from its initial value of 20 ms^{-1} (Fig. 5a), a reduction of just over 63%. Zonal counter currents ($u' < 0$) of magnitude ~ 2 ms^{-1} exist north (south) of the main jet core, which may be viewed as portions of perturbation return flow around the centers of low (high) pressure becoming established in these regions (Fig. 5d) as the thermodynamic fields (p' and θ') adjust to the nondivergent portion of the perturbation

winds. The horizontal structure of θ' is similar to p', and the vertical structures are related hydrostatically ($1/\rho_0 \partial p'/\partial z = g\theta'/\theta_0$). At this time transient inertia-gravity waves are also evident in the evolving geostrophic winds (not shown), and are associated with the zonal ($v'_g = 1/(\rho_0 f)\partial p'/\partial x$) and meridional ($u'_g = - 1/(\rho_0 f)\partial p'/\partial y$) gradients of the evolving perturbation pressure field (Fig. 5d).

Within the context of linear theory, no contribution from the initial PV anomaly $q'_i = - \partial u_{jet}/\partial y$ is partitioned to the vertical velocity field, whose response consists totally of transient dispersive inertia-gravity waves (Fig. 5c) yielding, in the balanced equilibrium state, a field of absolutely no vertical motion (not shown). The steady-state response which conserves PV is a nondivergent geostrophic zonal jet with confluent (diffluent) flow in its entrance (exit) region, supported by a dipole pressure couplet, with centers of cold (warm) air colocated with the center of low (high) pressure at all levels below the level of maximum zonal wind. Centers of warm (cold) air are colocated with the perturbation low (high) pressure centers north (south) of the jet core at all levels above the level of maximum zonal wind. The absolute magnitudes of the steady-state u', v', p', and q' fields are 9.32 ms^{-1}, 2.2 ms^{-1}, 0.27 mb, and 0.098 K, respectively. This steady-state equilibrium defines a *thermal wind balance among the baroclinic perturbations* throughout the depth of the unbounded Boussinesq atmosphere.

Fig. 6 shows the results seen by a Galilean observer traveling at the speed $c < U$ at t = 12 h after a traveling zonal momentum forcing whose horizontal and vertical structure given by

$$F_x = U^* \frac{\partial}{\partial x} [u_{j0} \{ \frac{(x-ct)^2}{a^2} + \frac{y^2}{b^2} + 1 \}^{-3/2}] e^{- z^2/d^2} \qquad (14)$$

is introduced into the basic state flow. This applied forcing is chosen to represent *the effect of inertial-advective acceleration the barotropic current* (which is itself taken to be representative of the midlatitude jet stream) *experiences as it passes through the slower moving quasi-steady jet*

streak. The zonal and meridional half-widths a and b are equal to 500 km, the e-folding half-depth d = 12.5 km, u_{j0} = 30 ms^{-1}, and U* = U-*c*, where U = 20 ms^{-1} and *c* = 10 ms^{-1}. The significant radius of deformation for this case is $L_R = N(2d)/f$ = 2500 km, which is comparable to that of a homogeneous atmosphere of finite depth whose surface temperature is approximately 273 K. Since $a = b = L_R/5 << L_R$, we can expect the thermodynamic fields to adjust to the externally forced wind fields.

At this time the zonal wind field has a structure resembling that of the applied forcing of absolute magnitude ~ 5ms^{-1} due to the imposed initial condition $\partial u'_i/\partial t = F\xi$ (Fig. 6a). The meridional wind field is dominated by localized southerly (northerly) flow of comparable magnitude north (south) of the forcing center (Fig. 6b), and can be attributed to the horizontal gradient of the evolving p' field at this level (Fig. 6d). Note that the perturbation pressure field has a markedly 'four-cell' pattern at this time which is related to a transfer of mass from the cyclonic to the anticyclonic (anticyclonic to the cyclonic side) in the entrance (exit) region of the traveling momentum forcing associated with the meridional ageostrophic winds v'_a which exist in these regions (not shown). This mass adjustment causes a 'four-cell' pattern of vertical motion to be set up in the quadrants flanking the localized momentum forcing (Fig. 6c), with rising (sinking) motion in the northwest and southeast (southwest and northeast) quadrants.

By t = 48 h, the zonal counter current (u' < 0), portions of the meridional wind field, and the high-low p' dipole which were located in the exit region of the applied forcing are being advected downstream at the relative velocity U-*c* by the basic state flow (not shown), and are the PV anomaly generated by the external momentum forcing. The steady-state equilibrium (not shown) consists of a quasi-geostrophically balanced zonal jet streak with confluent (diffluent) flow in its entrance (exit) region, supported by a dipole couplet of low (high) perturbation pressure north (south) of the jet core. A dipole couplet of cold (warm) air whose center is colocated with the center of low (high) p' exists at all levels below the level of maximum zonal wind. This θ' field is reversed at levels above the jet core, whose horizontal gradients support the vertical shear of

the zonal and meridional wind perturbations establishing thermal wind balance throughout the rotating Boussinesq atmosphere.

4. Conclusions

4.1 Initial Value Problem

- The initial PV anomaly governing the evolution in the geostrophic wind perturbations is given by the meridional gradient of the ageostrophic jet, $q'_i = - \partial u_{jet}/\partial y$.

- The initial zonal acceleration ($\partial u'_i/\partial t$) is due to the linear advection of the ageostrophic zonal jet by the basic flow ($-Du_{jet}/Dt$), and the initial meridional acceleration ($\partial v'_i/\partial t$) is associated with the Coriolis force acting on the unbalanced PV state.

- The steady-state equilibrium which conserves PV is a geostrophic zonal jet with meridionally confluent (diffluent) flow in its entrance (exit) region, supported by a dipole couplet of perturbation low (high) pressure north (south) of the jet core.

- Zonal counter currents ($u' < 0$) exist north and south of the main jet, and are portions of the perturbation return flow around the pressure couplet supporting the geostrophic jet.

- The geostrophic zonal jet is advected downstream by the basic state flow, establishing the physical mechanisms of geostrophic vorticity ($-\mathbf{U}\cdot\nabla\zeta'_g$) and horizontal temperature ($-U\cdot\nabla\theta'$) advection.

- Linear theory predicts the preservation in both magnitude and geometry of a geostrophically balanced zonal jet streak introduced into both homogeneous and continuously stratified barotropic flows.

4.2 Forced Problem

- A PV anomaly is advected downstream at the relative velocity U-c, with steady-state geostrophic and ageostrophic circulations confined to the forcing region.

- For $t \leq \tau = 2a/(U-c)$, the zonal wind perturbation is similar in horizontal and vertical structure to the applied forcing since $\partial u'_i/\partial t = F\xi$. For $t > \tau$, the downstream advection of the PV anomaly generated by the external forcing dominates the perturbation response.

- For forcing geometry representative of the alongstream gradients of midlatitude jet streaks, the linear steady-state response is a zonally localized quasi-geostrophic (QG) jet streak.

- The external momentum forcing can either (i) enhance, (ii) destroy, or (iii) reinforce the PV associated with the initial disturbance.

4.3 Effects of Nonlinearity

- Theoretical analysis of the nonlinear QG field equations indicates that in a rotating Boussinesq flow, a four-cell pattern of vertical motion exists in the quadrants flanking the zonal jet core, consistent with that of real midlatitude jet streaks.

- Thermally direct (indirect) ageostrophic circulations exist in the entrance (exit) region at levels below the jet core, while thermally indirect (direct) circulations exist in the entrance (exit) region above the jet core which preserve the local thermal wind balance.

- In a rotating homogeneous atmosphere, the four-cell pattern of vertical motion is simply reversed due to the constraints imposed by Taylor-Proudman mass continuity.

5. Acknowledgements

This research is funded under NSF Grants ATM-8815180, ATM-9224595, and the NASA Grant NAG5-1790. Simulations were performed on the Cray Y-MP at NCSC and the IBM FOAM^{V} workstations at NCSU.

6. References

Cahn, A., 1945: An investigation of the free oscillations of a simple current system. *J. Meteor.*, **2**, 113-119.

Kaplan, M. L., R. A. Rozumalski, R. P. Weglarz, Y.-L. Lin, and S. E. Koch, 1994a: Numerical simulation studies of the role of convectively-driven ageostrophic jet streak adjustments in creating a favorable environment for the development of an isolated tornado outbreak. *Preprints*, 6th AMS Conf. on Mesoscale Processes, 18-22 July, 1994, Portland, Oregon, 144-146.

-------, S. E. Koch, Y.-L. Lin, R. P. Weglarz, and R. A. Rozumalski, 1994b: The numerical simulation of meso-beta scale geostrophic adjustment processes resulting in secondary upper/lower-level jet formation and internal gravity waves during CCOPE. *Preprints*, 6th AMS Conf. on Mesoscale Processes, 18-22 July, 1994, Portland, Oregon, 382-384.

Rossby, C. G., 1938: On the mutual adjustment of pressure and velocity distributions in simple current systems, 2. *J. Mar. Res.*, **1**, 239-263.

Weglarz, R. P., 1994: Three-dimensional geostrophic adjustment of homogeneous and continuously stratified atmospheres with application to the dynamics of midlatitude jet streaks. Ph.D. dissertation, Department of Marine, Earth, and Atmospheric Sciences, North Carolina State University, 414pp.

List of Figures

Figure1: GMASS simulation A of 500 mb wind vectors (alternate grid points) and isotachs (ms^{-1}) valid at (a) 0000 UTC, and (b) 0600 UTC 11 July 1981.

Figure 2: GMASS simulation A of 500 mb height (solid in m) and temperature (dashed in C) valid at (a) 0200 UTC and (b) 0800 UTC, and 500 mb omega (micb s^{-1}) valid at (c) 0500 UTC 11 July 1981. Indirect circulation cells denoted by "T".

Figure 3: GMASS simulation A of (a) 500 mb wind vectors (alternate grid points) and isotachs (ms^{-1}) and (b) 500 mb omega (micb s^{-1}) both valid at 1300 UTC 11 July 1981.

Figure 4: GMASS simulation B of 500 mb omega (micb s^{-1}) valid at 1300 UTC 11 July 1981. Gravity wave troughs and ridges occur along nodal surfaces in the vertical motion fields (denoted by "T" and "R", respectively).

Figure 5: Linear theoretical response of an unbounded rotating Boussinesq atmosphere at t = 6h to the impulsive addition of localized zonal momentum.

Figure 6: Linear theoretical response of an unbounded rotating Boussinesq atmosphere at t = 12h as seen by a Galilean observer traveling at the speed $c < U$ due to the propagating zonal momentum forcing given by Eq. (14).

Publications Resulting from the Research Project During FY94

Kaplan, M. L., S. E. Koch, Y.-L. Lin, R. P. Weglarz, and R. A. Rozumalski, 1994: The numerical simulation of meso-beta scale geostrophic adjustment processes resulting in secondary upper/lower-level jet formation and internal gravity waves during CCOPE. *Preprints*, 6th AMS Conf. on Mesoscale Processes, 18-22 July, 1994, Portland, Oregon, 382-384.

Weglarz, R. P., 1994: Three-dimensional geostrophic adjustment of homogeneous and continuously stratified atmospheres with application to the dynamics of midlatitude jet streaks.

Ph.D. dissertation, Department of Marine, Earth, and Atmospheric Sciences, North Carolina State University, 414pp.

-------, and Y.-L. Lin, 1994a: Geostrophic adjustment and jetogenesis forced by impulsive and propagating zonal momentum sources in a rotating atmosphere. *Preprints*, 6th AMS Conf. on Mesoscale Processes, 18-22 July, 1994, Portland, Oregon, 324-327.

-------, and -------, 1994b: Geostrophic adjustment and jetogenesis forced by impulsive and propagating zonal momentum sources. Part I. Three-dimensional response of a rotating homogeneous atmosphere of finite depth. Submitted to *J. Atmos. Sci.* for publication.

Abstract

This paper examines a likely mechanism for the organization of the second gravity wave episode observed by Koch *et al.* (1988) over the CCOPE mesonet in eastern Montana. Numerical simulation results as well as lower tropospheric observations indicate that shortly after the mid-upper tropospheric geostrophic adjustment process described in Kaplan *et al.* (1994, Part I), a diurnal circulation was developing upstream over the Rocky Mountains which encompassed the origin location of the second gravity wave episode.

The diurnal circulation represented a classic mountain-plains solenoid, where the early morning solar heating of the elevated plateau over the wave generation region produced a lower-middle tropospheric thermally-direct circulation. The rising branch of this circulation developed in response to the heating of the planetary boundary layer by surface sensible heat flux during the morning. The sinking branch of the circulation extended downstream over the lower plains region as mass processed though the ascending branch sank in the cooler air far from the elevated plateau. The significance of this mountain-plains solenoidal circulation for gravity wave generation lies in the fact that above the inflowing branch of the thermally-direct circulation within the boundary layer is an outflowing jet of air extending downstream. This diabatically-induced outflow jet acts to produce a source of lower-middle tropospheric momentum which impulsively perturbs the mass-momentum balance as well as the vertical Scorer Parameter structure just downstream of the mountains over the wave generation region. Hence, it acts like its predecessor low-level jet, diagnosed from numerical simulation studies in Part I, which was primarily the result of adiabatic geostrophic adjustment processes accompanying the polar jet streak, in that it impulsively perturbs the mesoscale mass field which itself is undergoing differential terrain-induced diabatic heating.

This case study of mountain-plains solenoid development is unique from other published case studies because of this *unseasonably strong background mid-upper tropospheric jet streak directly above the mountain-plains region.* All other published two and three-dimensional simulation studies of the mountain-plains solenoidal circulation employed background atmospheric states which were largely synoptically calm, i. e., large anticylonic patterns devoid of strong jet streaks, therefore largely devoid of strong vertical wind shears. The background zonal momentum accompanying the mid-upper tropospheric jet streak in the CCOPE case study acts to increase the magnitude of the outflowing mid-lower tropospheric jet which effectively acts to increase the mass fluxes accompanying the mountain-plains solenoidal circulation. The stronger low-level jet structure simply aids in the impulsive organization of mass perturbations which eventually amplify into internal gravity waves. Thus, a second low-level jet is coupled to a second episode of gravity waves during CCOPE. The upper-level jet implicitly enhances the gravity wave generation process by providing additional momentum to accelerate the nonlinear increase in velocity divergence during the geostrophic adjustment of the wind field to the perturbed mass above the heated elevated plateau.

As was the case in Part I accompanying the first gravity wave episode, this second low-level jet and geostrophic adjustment process establishes the initial slowly propagating wave perturbations which eventually amplify into rapidly-propagating inertia-gravity waves when latent heating perturbs the vertical wave structure.

Abstract

We extend the recent results of Weglarz and Lin (1994, Part I) by investigating the three-dimensional linear response of a zonally uniform barotropic flow in a vertically unbounded, continuously stratified, Boussinesq atmosphere. The methods of perturbation potential vorticity (PV) theory are used to address the initial-value and forced geostrophic adjustment problems imposed by (i) the introduction of an unbalanced zonal wind anomaly into the geostrophically balanced basic state flow, and (ii) a traveling zonal momentum forcing in the interior of the fluid, respectively.

The transient response shows evidence of dispersive IGWs which excite a broader spectrum of modes in the zonal direction as compared to the meridional direction. The dispersive IGWs in all fields are essentially removed in the first 12 h of the response associated with the initial-value problem. The existence of a uniform zonal flow Doppler shifts the phase velocities of the transient IGWs responsible for removing the ageostrophic divergence of the initial state during the adjustment to geostrophic equilibrium. The steady-state response predicted by linear theory which conserves the PV of the initial state is a localized, geostrophic zonal jet with meridionally confluent (diffluent) flow in its entrance (exit) region, which is supported by a couplet of perturbation low (high) pressure north (south) of the zonal jet core. The steady-state linear response characterizes a localized *thermal wind balance* among the baroclinic perturbations defining the primary circulations associated with the geostrophic jet. In the absence of momentum forcing, the secondary circulations predicted by linear theory are trivially zero. In a non-zero basic state flow, the steady-state PV couplet is advected downsteam by the uniform zonal flow.

Taking the basic flow to be locally representative of the planetary jet stream in which midlatitude jet streaks are observed to exist, we investigate the response to a momentum forcing propagating at the speed $c < U$ through the basic state current. The magnitude of the traveling zonal wind anomaly represented by this forcing is taken to be greater than the magnitude of the basic state flow, $| u_{j0} | > | U |$, yielding propagation characteristics very representative of real midlatitude jet streaks.

For a Galilean observer, the response predicted by linear theory at early times is primarily dominated by the prescribed structure of the imposed momentum forcing. Since the length scale of the forced zonal winds are much less than the Rossby deformation radius defined by the total depth of the zonal wind anomaly represented by the forcing ($L_R \sim N2d_{jet}/f$), the transient response associated with this particular forced adjustment problem shows the adjustment of the mass fields to the momentum (wind) fields. At later times, the linear response is dominated by the circulations associated with the PV anomaly generated by the meridional gradient of the 'vorticity' of the prescribed forcing, $-\partial F_\zeta/\partial y$.

An isolated zonal jet with meridionally confluent (diffluent) flow in the jet entrance (exit) region eventually becomes established in the vicinity of the forcing center. A dipole couplet of perturbation pressure supports this localized zonal jet. This pressure couplet is related hydrostatically to the perturbation potential temperature field. The forced geostrophic circulations are similar to that predicted for the initial-value problem. The ageostrophic circulations transfer mass from the cyclonic to the anticyclonic (anticyclonic to the cyclonic) side of the jet core in the entrance (exit) region, yielding a well-defined 'four-cell' pattern of vertical motion in the quadrants flanking the jet core. These transverse ageostrophic circulations are similar to those produced in a rotating homogeneous atmosphere of finite depth, but are simply *reversed* from those commonly inferred to be associated with midlatitude jet streaks in the real atmosphere. We define the forced linear response as baroclinic *jetogenesis*.

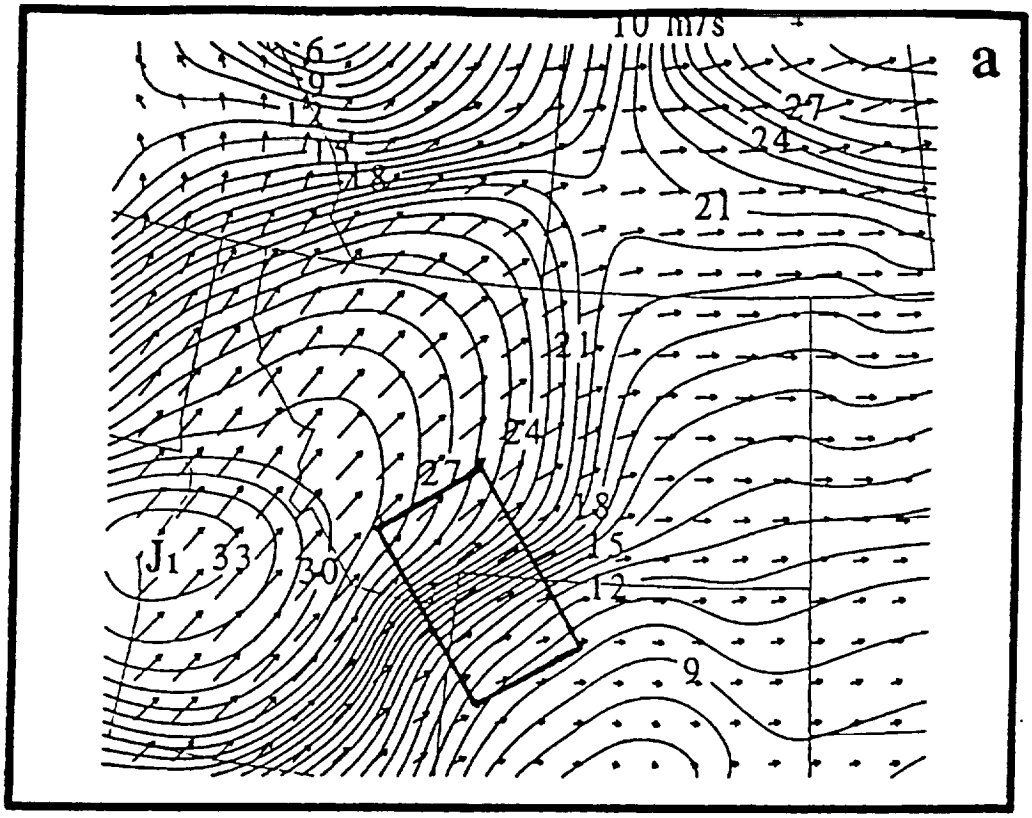
10 m/s
a
6
9
12
15
18
21
24
27
J1
33
30
27
24
21
18
15
12
9

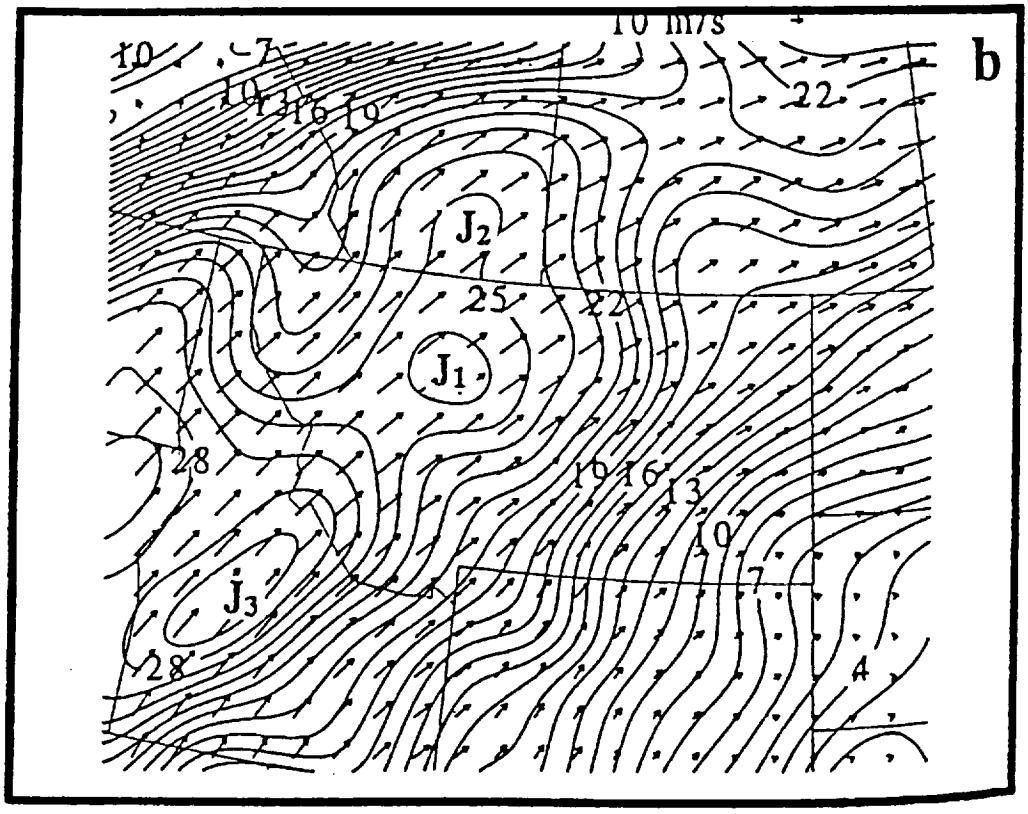
10 m/s
b
10
7
10
13
16
19
22
J2
25
22
J1
28
19
16
13
10
7
J3
28
4

Figure 1

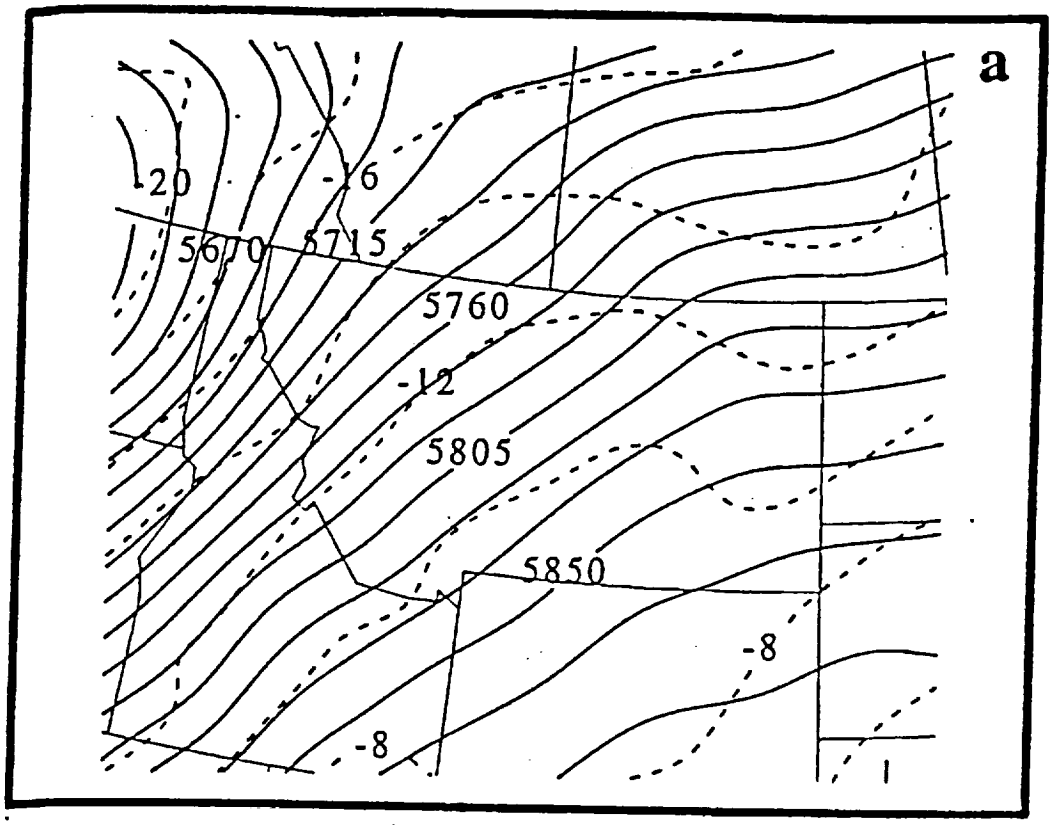
a
-20
-6
5670
5715
5760
-12
5805
5850
-8
-8

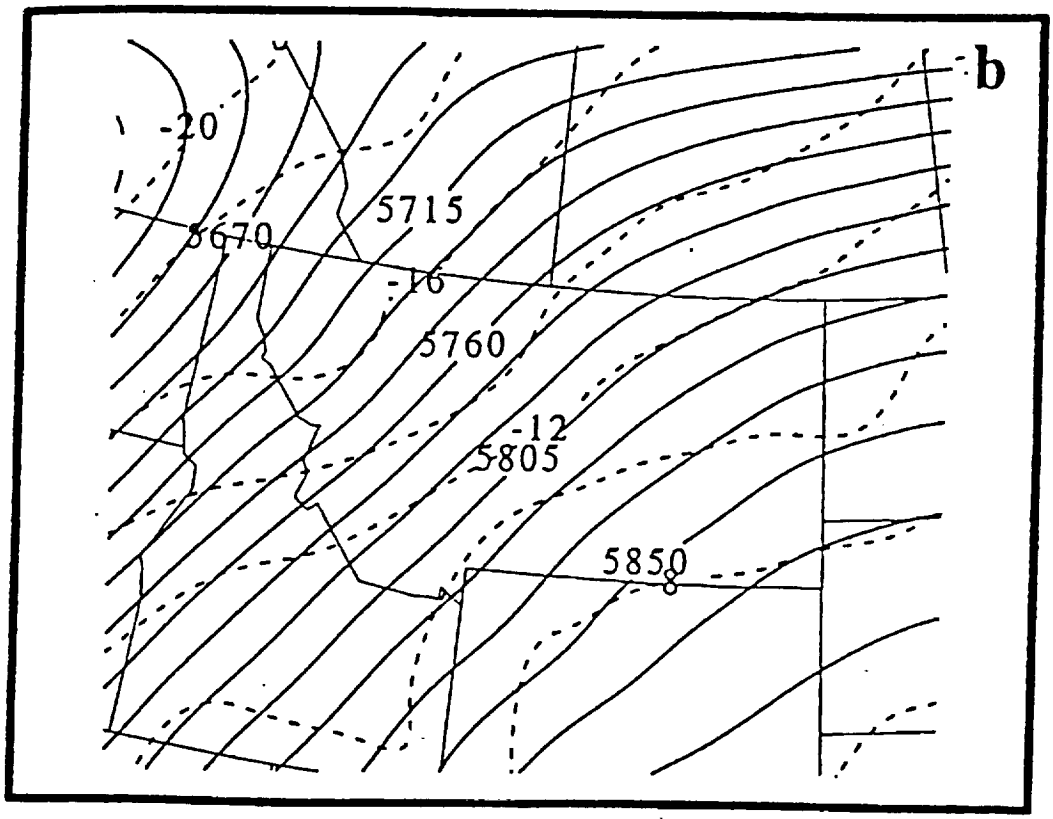
b
-20
5715
5670
-16
5760
-12
5805
5850
8

Figure 2

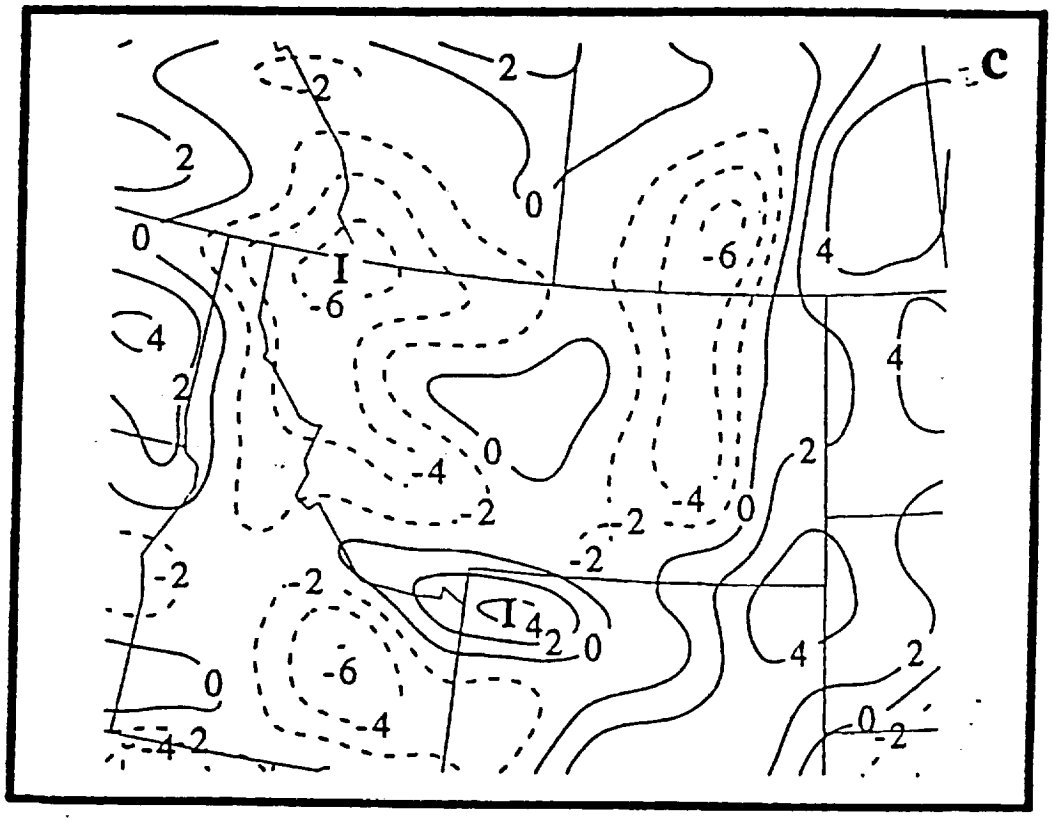

Figure 2

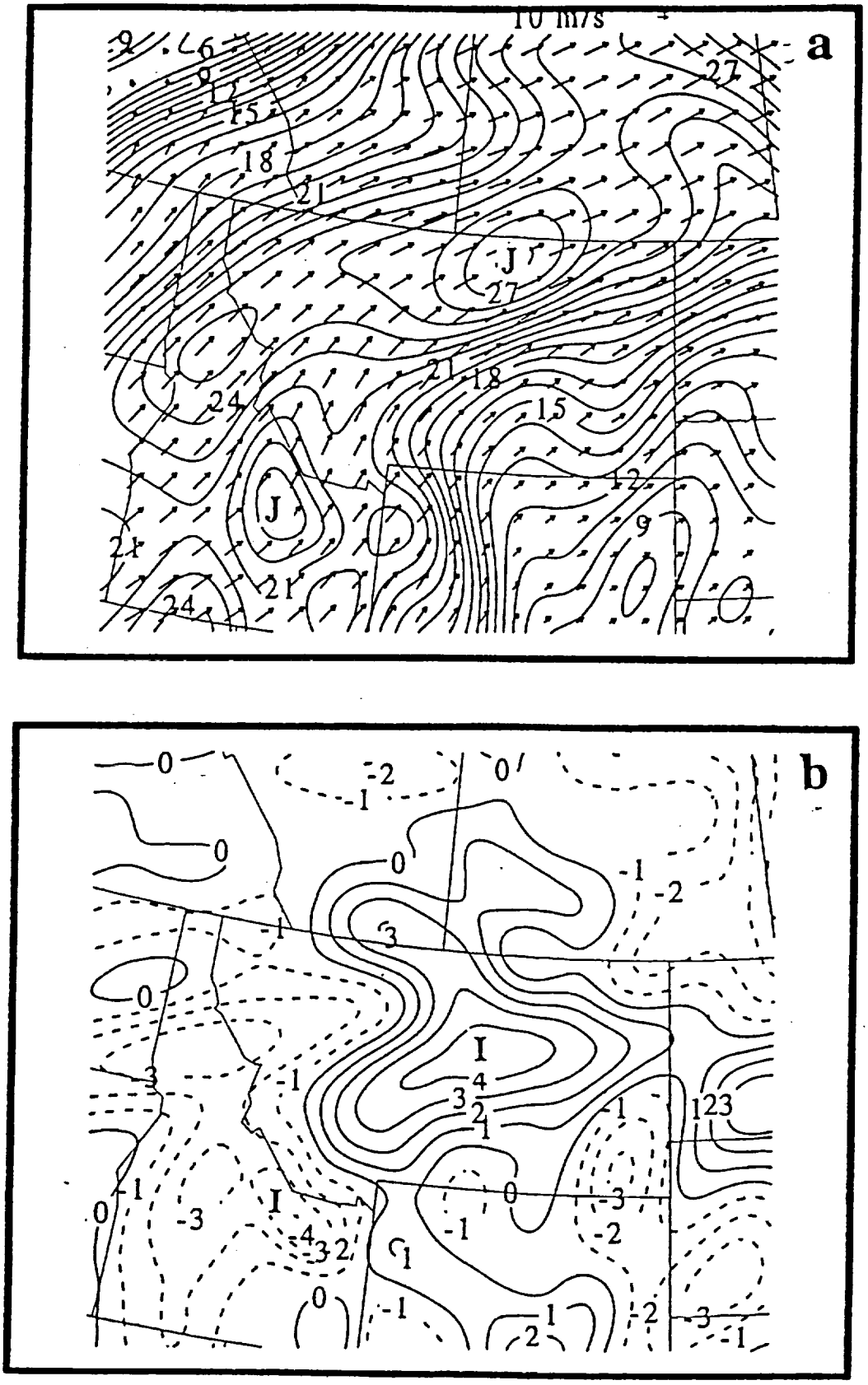

Figure 3

Figure 4

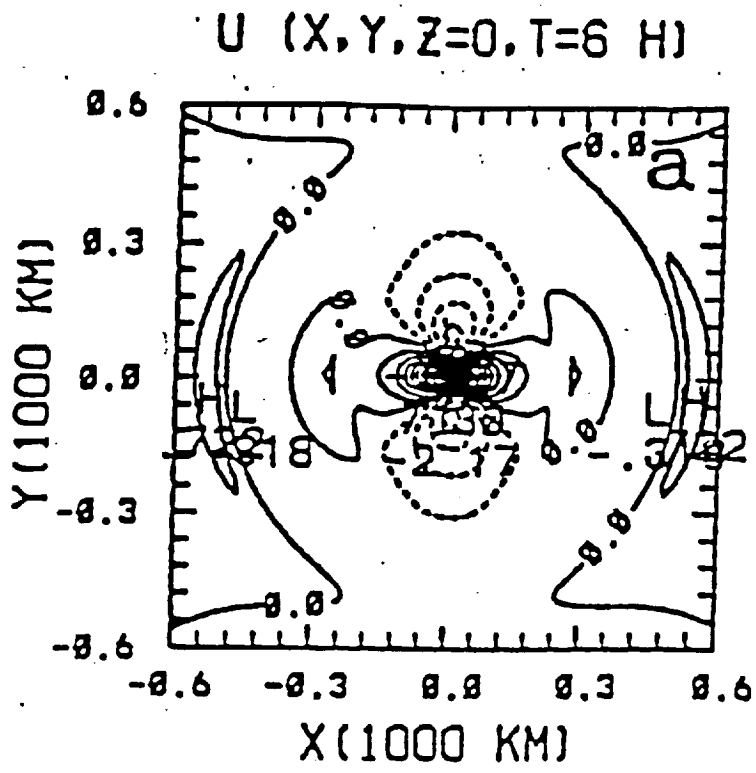
U (X, Y, Z=0, T=6 H)
a
0.0
0.0
0.0
0.0
0.6
0.3
0.0
-0.3
-0.6
Y(1000 KM)
-0.6
-0.3
0.0
0.3
0.6
X(1000 KM)

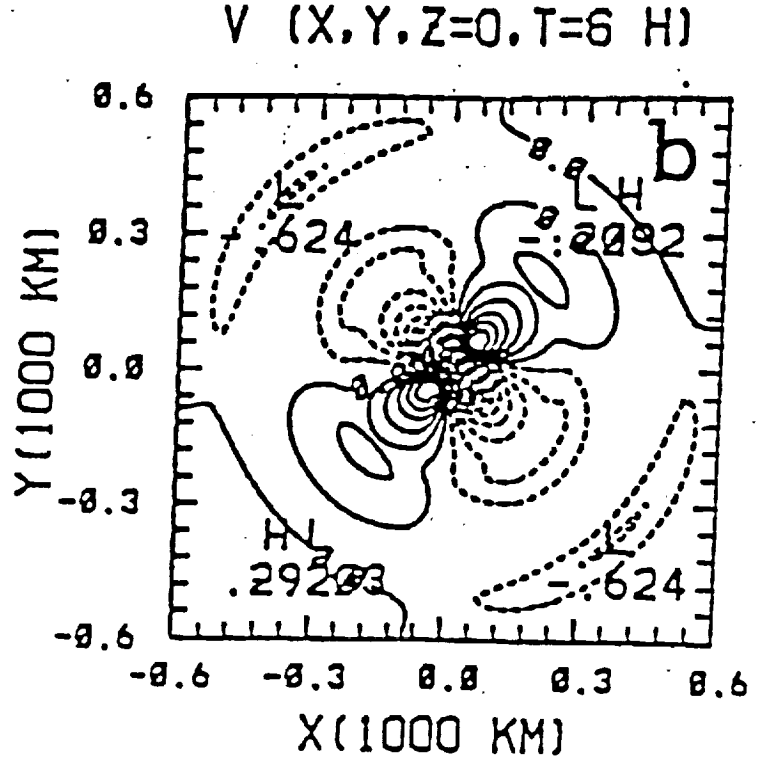
V (X, Y, Z=0, T=6 H)
b
0.0
0.6
0.3
0.0
-0.3
-0.6
Y(1000 KM)
-0.6
-0.3
0.0
0.3
0.6
X(1000 KM)

Figure 5

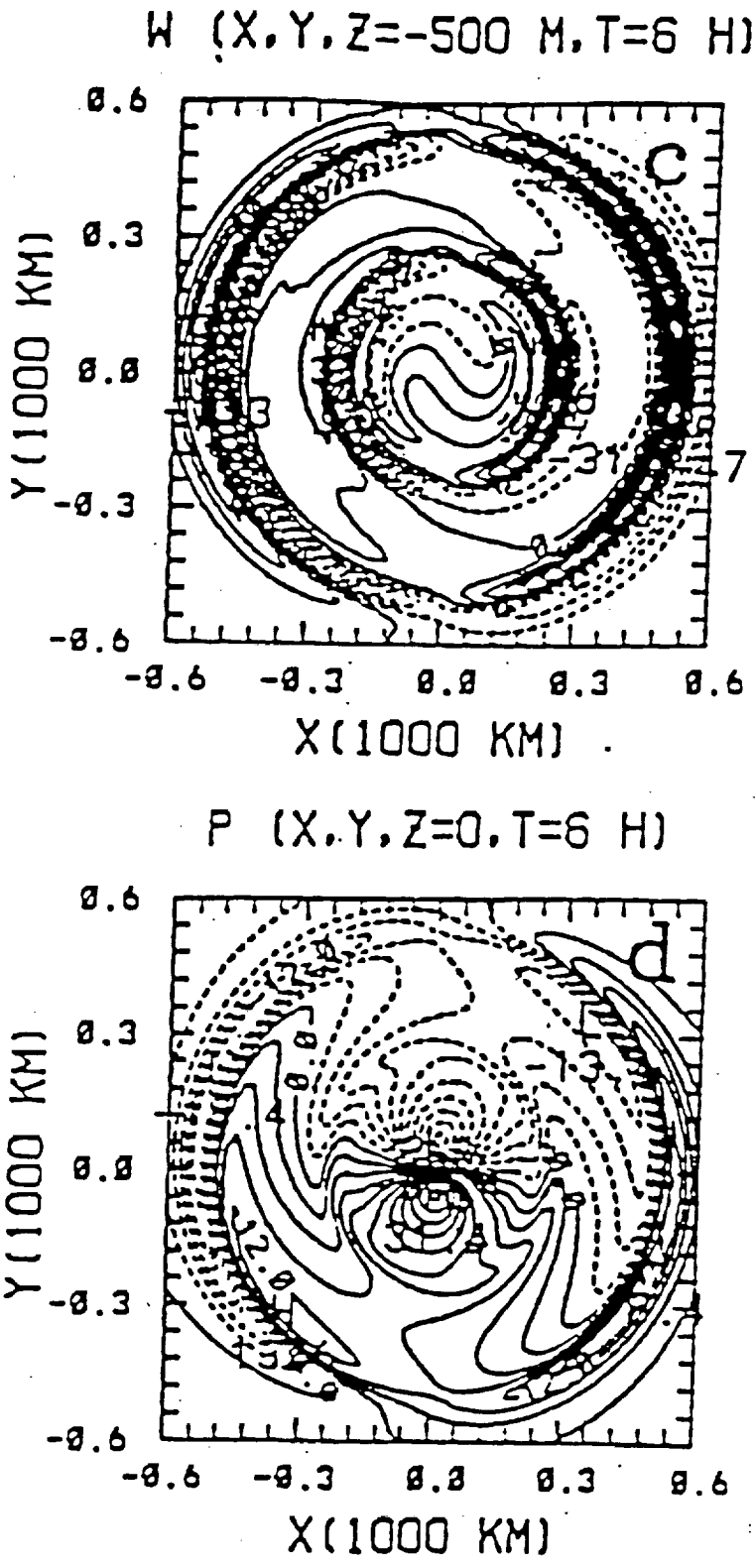
W (X,Y,Z=-500 M,T=6 H)
C
-3
7
Y(1000 KM)
X(1000 KM)
0.6
0.3
0.0
-0.3
-0.6
P (X,Y,Z=0,T=6 H)
D
0.8
-2.0
-3.0

Figure 5

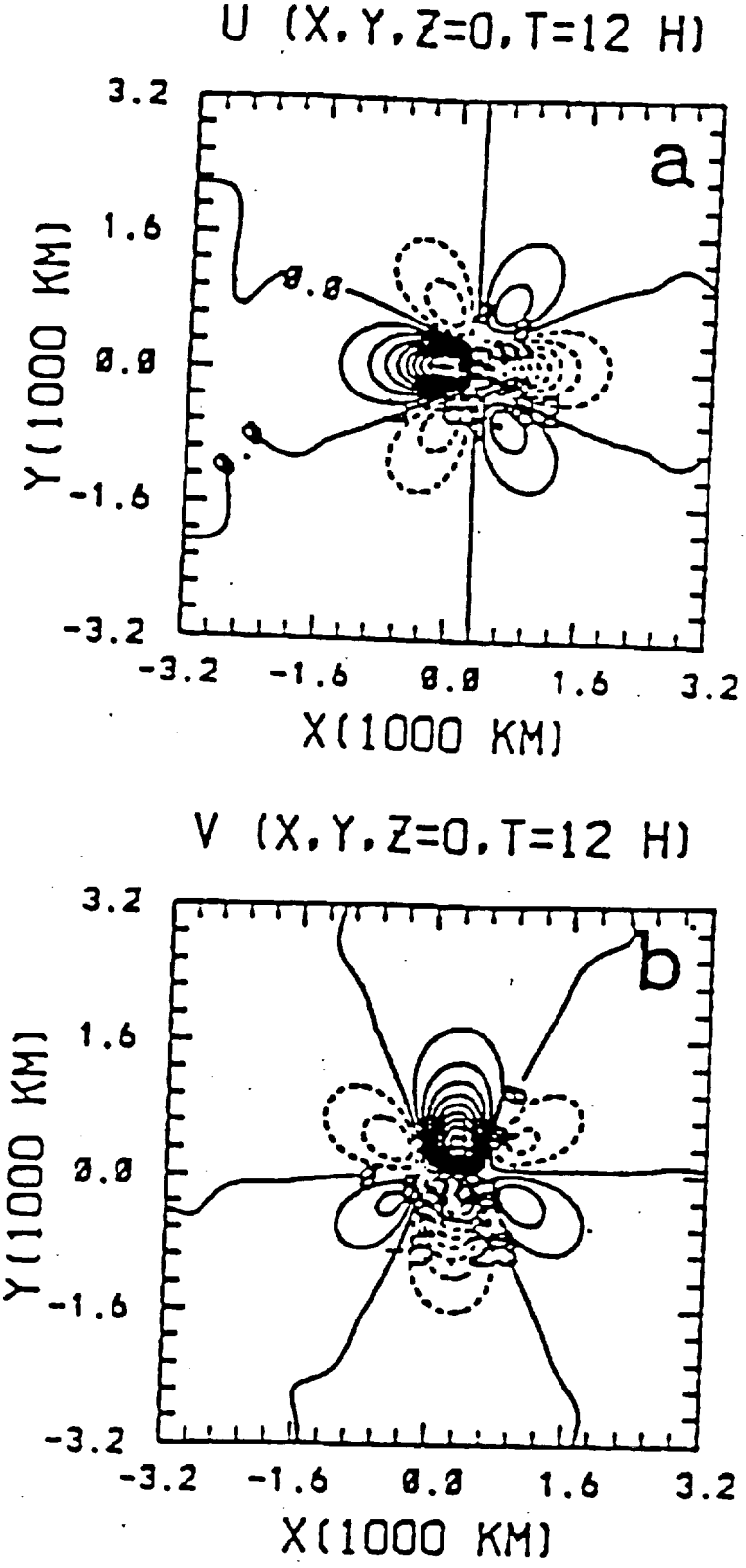
U (X, Y, Z=0, T=12 H)
a
3.2
1.6
0.0
-1.6
-3.2
Y(1000 KM)
-3.2 -1.6 0.0 1.6 3.2
X(1000 KM)
V (X, Y, Z=0, T=12 H)
b
3.2
1.6
0.0
-1.6
-3.2
Y(1000 KM)
-3.2 -1.6 0.0 1.6 3.2
X(1000 KM)

Figure 6

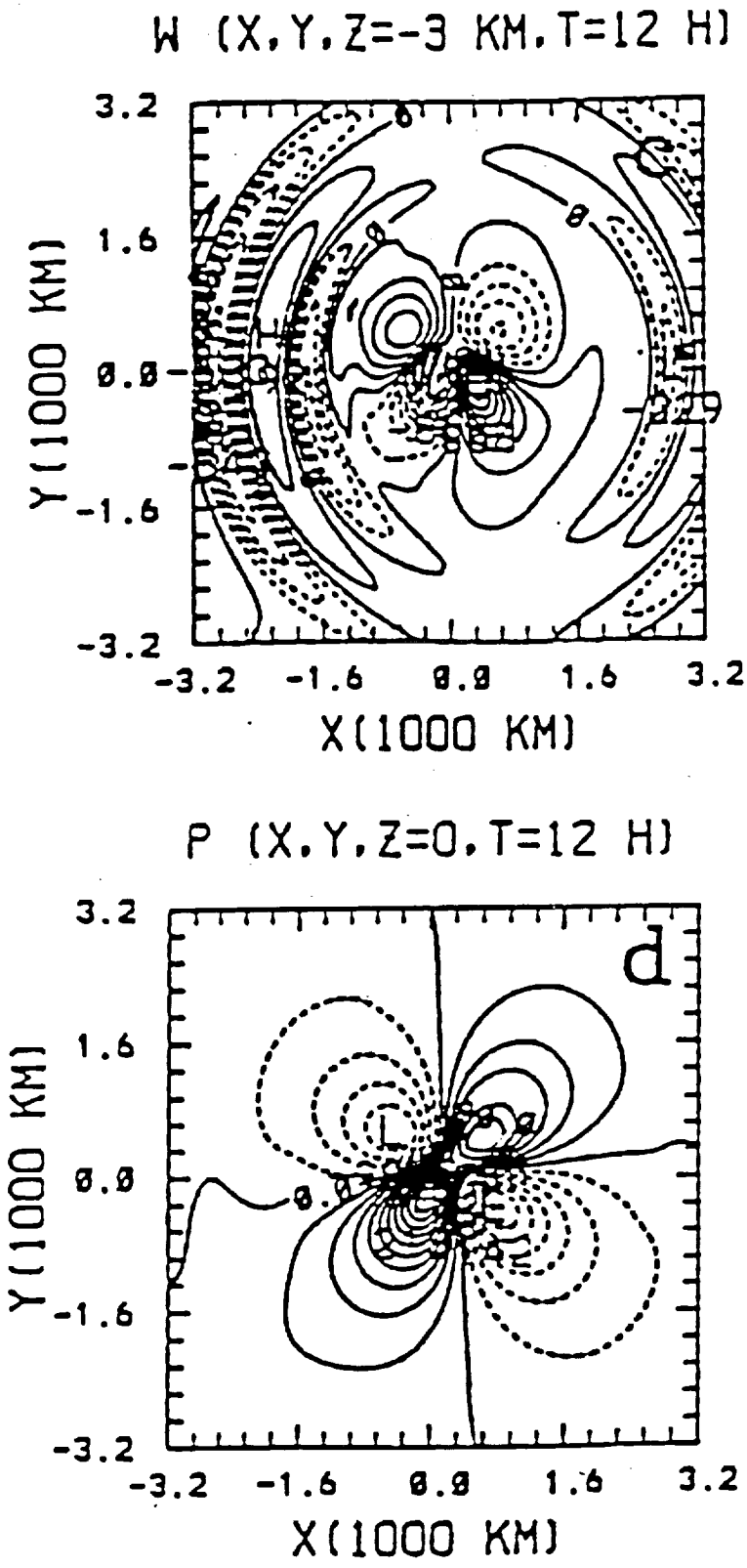
W (X,Y,Z=-3 KM,T=12 H)
3.2
1.6
0.0
-1.6
-3.2
Y(1000 KM)
-3.2
-1.6
0.0
1.6
3.2
X(1000 KM)
P (X,Y,Z=0,T=12 H)
d
3.2
1.6
0.0
-1.6
-3.2
Y(1000 KM)
-3.2
-1.6
0.0
1.6
3.2
X(1000 KM)

Figure 6